BIOCHEMISTRY
including biophysical chemistry & molecular biology

Current Topic

pubs.acs.org/biochemistry

Molecular Architecture of the Bacterial Flagellar Motor in Cells

Xiaowei Zhao,[†] Steven J. Norris,[†,‡] and Jun Liu*[,†]

[†]Department of Pathology and Laboratory Medicine, University of Texas Medical School at Houston, Houston, Texas 77030, United States

[‡]Department of Microbiology and Molecular Genetics, University of Texas Medical School at Houston, Houston, Texas 77030, United States

ABSTRACT: The flagellum is one of the most sophisticated self-assembling molecular machines in bacteria. Powered by the proton-motive force, the flagellum rapidly rotates in either a clockwise or counterclockwise direction, which ultimately controls bacterial motility and behavior. *Escherichia coli* and *Salmonella enterica* have served as important model systems for extensive genetic, biochemical, and structural analysis of the flagellum, providing unparalleled insights into its structure, function, and gene regulation. Despite these advances, our understanding of flagellar assembly and rotational mechanisms remains incomplete, in part because of the limited structural information available regarding the intact rotor−stator complex and secretion apparatus. Cryo-electron tomography (cryo-ET) has become a valuable imaging technique capable of visualizing the intact flagellar motor in cells at molecular resolution. Because the resolution that can be achieved by cryo-ET with large bacteria (such as *E. coli* and *S. enterica*) is limited, analysis of small-diameter bacteria (including *Borrelia burgdorferi* and *Campylobacter jejuni*) can provide additional insights into the *in situ* structure of the flagellar motor and other cellular components. This review is focused on the application of cryo-ET, in combination with genetic and biophysical approaches, to the study of flagellar structures and its potential for improving the understanding of rotor−stator interactions, the rotational switching mechanism, and the secretion and assembly of flagellar components.

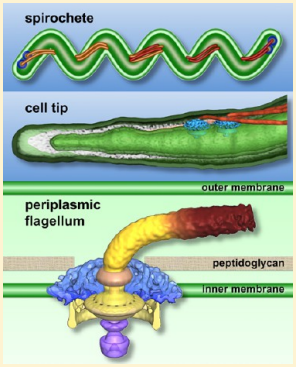

BACTERIAL MOTILITY AND FLAGELLA

Many bacteria require motility for their growth and survival. Motility is also essential for the infectivity of many prokaryotic pathogens. Although other types of motility exist (e.g., gliding motility), flagellum-mediated translational motion is the most common mechanism in bacteria.[1] Flagellar rotation is driven by the proton- or sodium-motive force across the cytoplasmic membrane. In most externally flagellated bacteria, counterclockwise rotation (CCW, as viewed from the distal end of the flagellum to where it inserts into the membrane) of the flagella results in bundling of the helical flagella and propulsion of the cell through liquid or viscous environments ("running"). The flagellar motor can reverse directions, as well, and when rotating clockwise (CW), the flagellar filaments separate, resulting in random motion of the cell with little translational movement ("tumbling"). A sophisticated chemotaxis signaling system allows the cell to sense chemical stimuli and transmit this information through a signal transduction cascade that regulates the direction of flagellar rotation.[2,3] Cells migrate in chemical gradients by biasing the three-dimensional (3D) random walk that is generated by the combination of run and tumble behaviors.[4]

SPIROCHETE AND PERIPLASMIC FLAGELLA

Spirochetes represent one of the major bacterial phyla and are unusual in both morphology and motility.[5] They are well-known for causing several diseases in both humans and animals, including Lyme disease (*Borrelia burgdorferi* and related organisms), relapsing fever (several *Borrelia* species), syphilis (*Treponema pallidum*), leptospirosis (*Leptospira* species), and swine dysentery (*Brachyspira* species).[5] Lyme disease is the most common vector-borne infection in the United States. Syphilis is a prevalent sexually transmitted disease in many areas of the world, while leptospirosis is the most common worldwide waterborne zoonosis.

B. burgdorferi is one of the best studied spirochetes in terms of motility.[5,10] In contrast to the external flagellar filaments found in most motile bacteria, spirochetes possess periplasmic flagella (PFs) that are enclosed between the outer membrane and the peptidoglycan layer within the periplasmic space (Figure 1). In *B. burgdorferi*, 7−11 PFs are inserted subterminally at both cell poles (Figure 1B). The PF bundles wind around a flexible protoplasmic cylinder and overlap in the middle of the cell.[6] The PFs are essential for the distinct morphology, motility, and infectious life cycle of *B. burgdorferi*.[6−9] The flagella at each end of the cell are coordinated to rotate in opposite directions during translational motion and in the same direction (i.e., either CW or CCW) during the spirochete equivalent of tumbling, called "flexing".[5,10] Rotation of the flagella causes a serpentine movement of the entire cell body, allowing the organism to efficiently bore its way through viscous media or tissue.

Received: January 14, 2014
Revised: March 30, 2014
Published: April 3, 2014

   dx.doi.org/10.1021/bi500059y | *Biochemistry* 2014, 53, 4323−4333

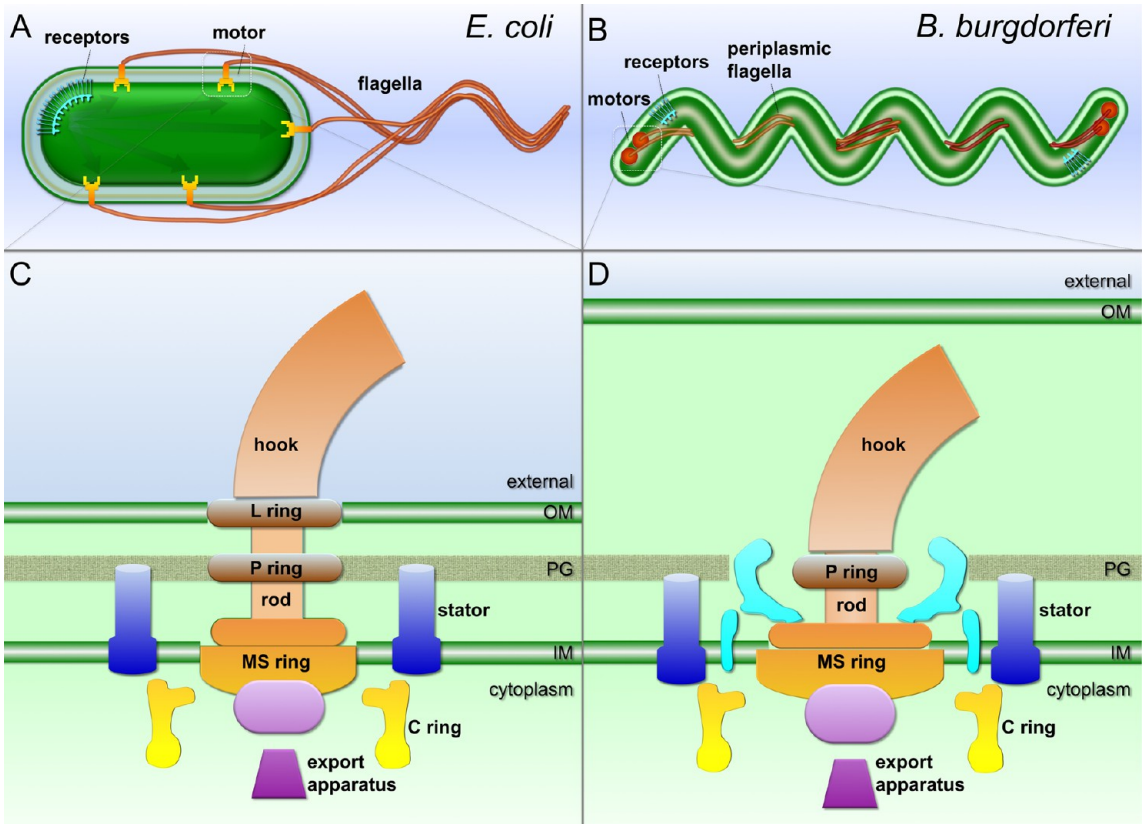

Figure 1. Schematic models of the external flagellum of *E. coli* (A and C) and periplasmic flagella of *B. burgdorferi* (B and D). Periplasmic flagella are distinct from the external flagella, as they are enclosed within the outer membrane and their flagellar motors are considerably larger and more complex. However, the core architecture of the two flagellar types is comparable. Shared structures include the MS ring, the C ring, the rod, the hook, the filament, the stator, and the export apparatus.

BACTERIAL FLAGELLAR MOTOR

The structure and function of bacterial flagella have been extensively studied in model systems *Salmonella enterica* and *Escherichia coli*, as summarized in several recent comprehensive reviews.[4,11−14] Of approximately 50 genes involved in the expression and assembly of the flagellum, ∼20 produce integral flagellar components. The flagellum consists of the motor, the hook, and the helically shaped flagellar filament (Figure 1A,B). The flagellar motor can be divided into several morphological domains (Figure 1C,D): the MS ring (FliF, the base for the flagellar motor), the C ring (FliG, FliM, and FliN, the switch complex regulating motor rotation), the export apparatus (a large complex exporting flagellar substrates), the rod (connecting the MS ring and the hook), the L and P rings on the rod (thought to serve as bushings at the outer membrane and at the peptidoglycan layer, respectively), and the stator, which is the motor force generator embedded in the cytoplasmic membrane.

The stator complex is composed of two transmembrane proteins, MotA and MotB, in *E. coli* and *S. enterica*. MotA has a large cytoplasmic domain, which contains conserved charged residues that are critical for the interaction with the rotor-associated protein FliG.[15,16] MotB has a large periplasmic domain that is believed to bind to the peptidoglycan layer.[17,18] The arrangements of MotA and MotB within the complex have been studied extensively by mutational analysis and systematic disulfide cross-linking studies.[19,20] Four MotA subunits and two MotB subunits form an ion-conducting complex ($MotA_4MotB_2$) that couples the proton flux to rotation of the rotor−flagellar filament assembly.[21] A conserved aspartic acid residue in the transmembrane segment of MotB (Asp32 in *E. coli*) is the predicted proton-binding site.[22] The proton binding or dissociation at this residue triggers conformational changes of the cytoplasmic domain of MotA in the stator, which are believed to drive the flagellar rotation through interactions between MotA and FliG.[23]

The flagellar export apparatus is responsible for the secretion of flagellar type III protein substrates, which include the polypeptide subunits of the flagellar rod, the hook, and the filament. The export apparatus uses both the ion-motive force[24,25] and the energy of ATP hydrolysis[26−28] to complete the export process. It is structurally and functionally homologous to the pathogenic type III secretion system (T3SS) that directly injects virulence factors into host cells.[29] The export apparatus is located at the bottom of the MS ring (Figure 1C,D) and is composed of six membrane proteins (FlhA, FlhB, FliP, FliQ, FliR, and FliO) and three soluble proteins (FliI, FliH, and FliJ) in the cytoplasm.[30] The membrane components are thought to form an export gate for secretion of the substrates, while the three soluble proteins form a FliH/FliI/FliJ complex that promotes the export process by binding and delivering export substrates to the export gate. It has been suggested that the FliH/FliI/FliJ complex has an architecture similar to that of F- and V-type ATPases.[31,32]

The structures of many flagellar proteins have been determined at atomic resolution, including components of the flagellar filament (FliC[33]), the C ring (FliM,[34] FliG,[35−37] FliN,[38] and the FliG/FliM complex[39,40]), and the stator (MotB[41,42]). Cryo-electron microscopy (cryo-EM) studies

dx.doi.org/10.1021/bi500059y | *Biochemistry* 2014, 53, 4323−4333

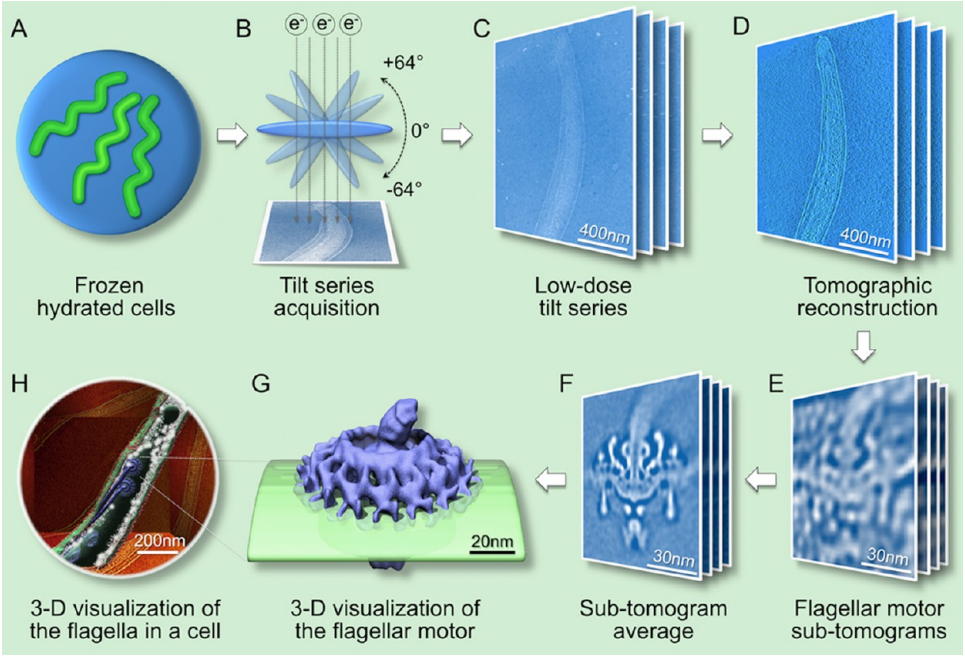

Figure 2. Workflow for determination of the *in situ* flagellar motor structure by cryo-electron tomography and subtomogram averaging. (A) Frozen hydrated specimen of a freshly prepared bacterial culture. (B) Cryo-EM images are collected by tilting the specimen from −64° to +64° in an electron microscope. (C) Low-dose tilt series of 2D projection images from a cell tip. (D) 3D reconstruction from a cell generated by backprojection. (E) Subtomograms containing the flagellar motor are extracted from tomographic reconstructions. (F) Thousands of the subtomograms are thoroughly aligned and averaged to determine the 3D structure at higher resolution. (G) 3D visualization of the intact flagellar motor embedded in the cytoplasmic membrane. (H) 3D visualization of a bacterial cell. Averaged motor structures are mapped back into the cellular context.

have provided the most detailed structures of the purified basal body, which contains the MS ring, the C ring, the rod, and the P and L rings.[43] However, these structures do not contain components of the stator and the export apparatus. In early electron microscopy studies, the stator and the export apparatus were visualized in freeze-fracture preparations of cytoplasmic membranes.[44−46] The first examination of the intact flagellar motor by cryo-electron tomography (cryo-ET) was reported in 2006.[47] This technique has been utilized to reveal the structural features of the stator and export apparatus in relation to the rotor elements.[48−52] The combination of high-throughput cryo-ET and genetic analysis has been particularly useful for dissecting flagellar motor structure and assembly at 3.5 nm resolution.[50,52,53] Therefore, this review is intended to provide an overview of this advanced imaging technique and its promising role in understanding the structure and function of intact flagellar motors.

3D VISUALIZATION OF INTACT FLAGELLAR MOTORS BY CRYO-ELECTRON TOMOGRAPHY AND SUBTOMOGRAM AVERAGING

Cryo-ET is a 3D imaging technique that in principle is comparable to computerized axial tomography (CAT) by which a 3D structure is reconstructed from its two-dimensional (2D) projections (Figure 2).[54] The unique strength of cryo-ET lies in its potential for visualizing large macromolecular assemblies in their native environment without fixation, dehydration, or staining artifacts. The preparation of frozen hydrated specimens is a critical step in this technique. Suspensions of freshly prepared, viable bacteria are deposited onto EM holey carbon grids and then rapidly frozen in liquid ethane at approximately −180 °C. Frozen hydrated specimens (Figure 2A) are then imaged at −170 °C using a cryo-electron microscope (Figure 2B). A low-dose tilt series of images (Figure 2C), which typically cover an angular range of −64° to +64° in 1.5° increments, is collected and aligned to generate a 3D tomographic reconstruction (Figure 2D).[52] The flagellar motors are readily visible in the reconstruction (Figure 2D). However, the resolution and contrast of one subtomogram from one flagellar motor are poor for fully understanding their molecular details (Figure 2E).

Subtomogram averaging and classification are the methods of choice for improving the signal-to-noise ratio and resolution of macromolecular assemblies.[55,56] Multiple copies of the flagellar motors are visually identified in the cell tomograms, and the 3D density map of each flagellar motor (Figure 2E) is extracted from its cellular context. Thousands of subtomograms are aligned and averaged to obtain a higher-resolution structure with an improved signal-to-noise ratio (Figure 2F,G). To minimize potential reference bias and also identify conformational heterogeneity, multivariate statistical analysis (MSA) is a key method utilized for the classification of subtomograms.[56,57] The resulting higher-resolution structures can be mapped back into their cellular context (Figure 2H), revealing the macromolecular organization at an unprecedented level.

Cryo-ET is a continuously evolving technique.[58,59] Many recent developments significantly enhance the resolution and throughput, including automation,[60] new methods for image processing,[61] phase-plate techniques,[62,63] and new generation direct electron detectors.[64,65] It is expected that employment of new technologies will greatly enhance the ability to determine higher-resolution structures of intact flagellar motors in a broader range of bacterial species.

dx.doi.org/10.1021/bi500059y | *Biochemistry* 2014, 53, 4323−4333

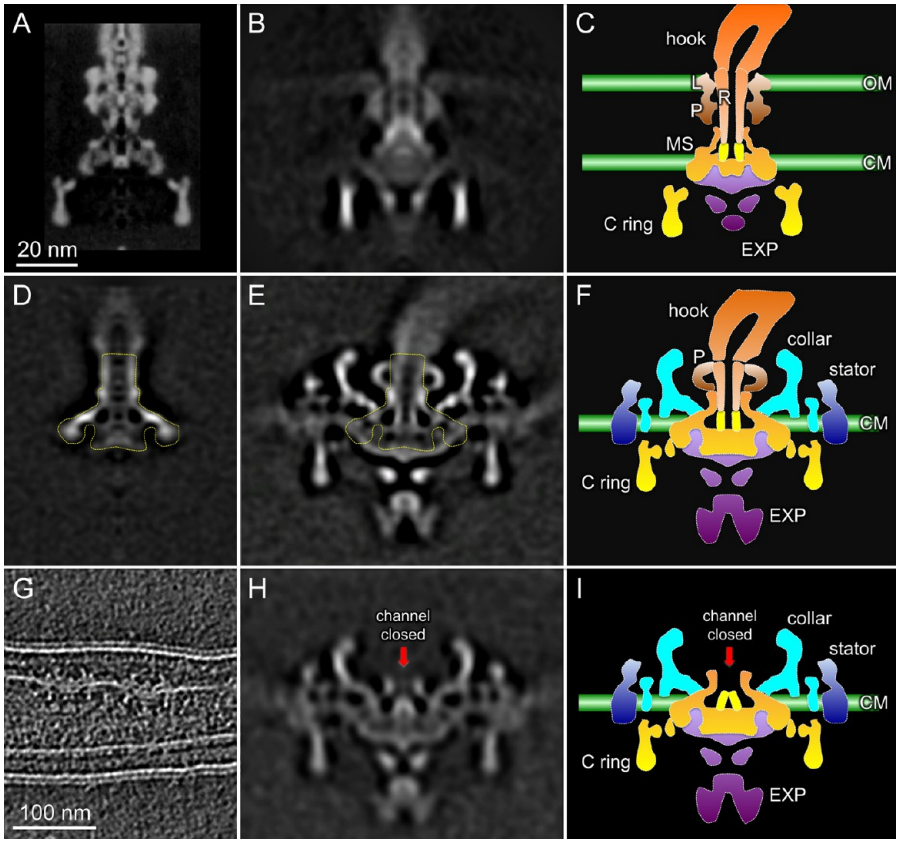

Figure 3. Comparative analysis of the intact motor and the purified basal body. (A) Purified *S. enterica* basal body structure determined by cryo-EM.[66] (B) *In situ S. enterica* motor structure reconstructed by cryo-ET.[49] (C) Cartoon model of the *S. enterica* flagellar motor. (D) The purified *B. burgdorferi* basal body structure determined by cryo-ET[50] is comparable to the MS ring and rod complex of the *S. enterica* basal body. (E) Intact motor structure of *B. burgdorferi*.[52] The basal body portion is outlined in the intact motor. (F) Cartoon model of the *B. burgdorferi* flagellar motor. (G) Slice from a cryotomogram of a Δ*fliE* mutant showing two flagellar motors lacking the filament and hook.[50] (H) Averaged motor structure of the Δ*fliE* mutant. The red arrow indicates that the central channel in the MS ring is closed. (I) Cartoon model of a rodless motor in the Δ*fliE* mutant. The architecture of the MS ring in the *B. burgdorferi* motor is similar to that of the MS ring in *S. enterica*.[67]

To fully understand the density maps derived from cryo-ET and subtomogram averaging, it is critical to fit ("dock") available atomic structures from individual components into 3D maps. Together with other structural and biochemical methods, cryo-ET is able to bridge the information gap from cells to molecules, which is essential for understanding the flagellar motor in its cellular context.

DIFFERENCES BETWEEN THE PURIFIED BASAL BODY AND INTACT FLAGELLAR MOTOR IN CELLS

Cryo-EM studies have provided a detailed structure of the purified basal body of *S. enterica*. However, many membrane-associated features are absent (Figure 3A),[66] as demonstrated by comparing basal body reconstruction with the low-resolution map derived from cryo-ET of *S. enterica* cells (Figure 3B).[49] Both membranes and the export apparatus are visible in the intact *S. enterica* motor, whereas little structural detail can be discerned in the stator region. In contrast, intact motor structures from relatively thin spirochetes, as exemplified by *B. burgdorferi* (Figure 3E,F), can be derived at higher resolution and reveal significantly more detail.[50,52] The intact *B. burgdorferi* motor structure is considerably more complex than its purified basal body (Figure 3D,E, basal body outlined). Many periplasmic and cytoplasmic components within the intact motor are dissociated during PF purification, including the unique periplasmic "collar", the stator, the P ring, the C ring, and the export apparatus. However, the remaining *B. burgdorferi* basal body is structurally comparable to the *S. enterica* basal body (minus the C ring), suggesting that it is composed of the MS ring and the rod.

The boundary between the rod and the MS ring has been defined by using cryo-ET reconstructions of a rodless *B. burgdorferi* Δ*fliE* mutant (Figure 3G).[50] In the absence of the rod, a socketlike domain of the MS ring is clearly revealed in the Δ*fliE* mutant (Figure 3H). As expected, the MS ring from *B. burgdorferi* shares a configuration similar to that in *S. enterica* (Figure 3I).[50,67] Notably, the central channel of the MS ring is closed in the Δ*fliE* motor (Figure 3H,I). In contrast, the channel is open in the intact motor, suggesting that the rod proteins form an integrated complex with the MS ring and thereby promote the opening of the channel (Figure 3E,F).

Comparative analysis of the *S. enterica* and *B. burgdorferi* motor structures allows definition of the conserved components in flagellar motor: the MS ring, the rod, the P ring, and the C ring (Figure 3C,F,I). It also provides guidance for the dissection of other components, which are not readily resolved by other approaches. Specifically, the combination of a large membrane-integrated domain and two cytoplasmic structures at the bottom of the MS ring is thought to be the export apparatus (Figure 3C,F,I, outlined in purple). In the *B. burgdorferi* motor, there is also a periplasmic structure, termed the collar (Figure 3F,I, outlined in cyan) that surrounds the MS ring, the P ring,

dx.doi.org/10.1021/bi500059y | *Biochemistry* 2014, 53, 4323−4333

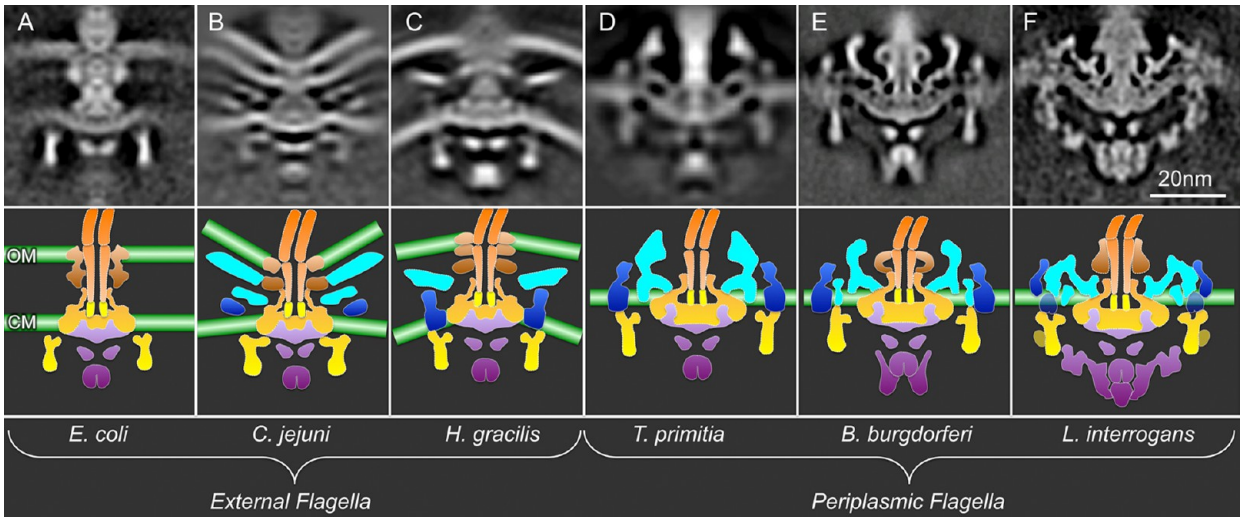

Figure 4. *In situ* flagellar motor structures from different organisms determined by cryo-ET and subtomogram averaging. (A−C) External flagella: *E. coli* (EMDB-5311), *C. jejuni* (EMDB-5300), and *H. gracilis* (EMDB-5309) flagellar motors. (D−F) Periplasmic flagella: *B. burgdorferi* (EMDB-5627), *T. primitia* (EMDB-1235), and *L. interrogans* (EMDB-5912−5914) flagellar motors.[51] The bottom panels show the corresponding cartoon models. The color scheme is the same as that in Figure 3. Noticeably, the densities of putative stator and export apparatus are clearly revealed in some bacterial species.

and the rod. This is a spirochete-specific structure, and the encoding genes have not been identified at the time of this review. Other peripheral densities that span the membrane are thought to represent the stators (Figure 3F,I, outlined in blue). In spirochetes, both the collar and the putative stators exhibit an evident 16-fold symmetry. Interestingly, the stator is embedded in a curved cytoplasmic membrane and reflects the same curvature; the intrinsic flexibility of the rotor−stator interaction is likely an important factor during flagellar rotation.[52]

INTACT MOTOR STRUCTURES IN DIFFERENT BACTERIAL SPECIES

Molecular architectures of intact flagellar motor from several phyla have been determined at 3−8 nm resolution by using cryo-ET and subtomogram averaging.[49,51,52,68] To illustrate the degree of conservation, six representative motor structures derived from several bacteria with external or periplasmic flagella are compared in Figure 4. The *E. coli*, *Campylobacter jejuni*, *Hylemonela gracilis*, and *Treponema primitia* motor structures were obtained in a comprehensive study by Chen et al.[49] Whereas the overall architectures vary between species,[49] the MS ring, the C ring, the rod, and the export apparatus have the same overall configuration as those determined in *S. enterica*[43] and *B. burgdorferi*,[50,52,68] suggesting that the core components of the flagellar motors and their interactions are conserved (Figure 4). In general, the MS ring forms the base of each motor. The socket and central channel of the MS ring are visible in all species, suggesting that it provides an evolutionarily conserved platform for rod assembly. The C ring is consistently attached to the cytoplasmic edge of the MS ring, but the C ring diameter varies considerably in different species. The export apparatus is located at the bottom of the MS ring. A doughnut-shaped torus is well conserved among different species and is located ∼6 nm below the inner membrane. Additional cytoplasmic densities likely correspond to the FliH/FliI/FliJ complex (Figure 4). Notably, the motor structures from *B. burgdorferi*[50,52] and *Leptospira interrogans*[51] reveal significantly more detail in the export apparatus and other components, which is thought to be due in part to the higher resolution that can be achieved with thin bacterial cells in combination with the use of a large number of individual motor structures for subtomogram averaging.

The rod functions as both the secretion channel and the drive shaft that transmits torque. Five proteins (FliE, FlgB, FlgC, FlgF, and FlgG) are involved in assembly of the rod.[69] When the rod proteins are effectively expressed, the central channel of the MS ring adopts an open conformation that serves as a template for rod assembly.[50] The proximal rod proteins assemble on top of the open channel of the MS ring in the following order: FliE, FlgB, FlgC, and FlgF.[50,69−71] The distal rod of external flagella is estimated to consist of four turns containing 26 FlgG subunits (∼15 nm in *S. enterica*).[70] In contrast, the distal rod (∼4 nm) in spirochetes is too short to penetrate the outer membrane (Figure 4E), contributing to the periplasmic localization of the flagella. It is likely that FlgG polymerizes in only one turn in *B. burgdorferi*, which appears to be the case for the other rod proteins (FlgB, FlgC, and FlhO, a FlgF homologue).[50] The variable rod length in species with external flagella is likely controlled by the degree of polymerization of the distal rod protein FlgG.

The P and L rings that are located around the rod of Gram-negative organisms are composed of FlgI and FlgH, respectively, and are thought to function as bushings in the cell envelope.[4,11] The densities on the external surface of the rod differ considerably in external flagella and periplasmic flagella (Figure 4), consistent with the variable presence of encoding genes *flgI* and *flgH*.[72] For example, *Treponema* species do not have identifiable *flgI* and *flgH* genes (Figure 4D) and lack both P and L rings.[47,73] *B. burgdorferi* has *flgI* but does not have *flgH*, consistent with the presence of the P ring, but not an L ring. Inactivation of *flgI* resulted in the loss of the P ring structure.[52] *L. interrogans* has both genes and has a large, contiguous density on the outer surface of the rod.[51] The exact functions of the rod-associated rings in spirochetes are not known.

The stator complexes (MotA/MotB) assemble around the MS ring in the cytoplasmic membrane. In *S. enterica* and *E. coli*,

dx.doi.org/10.1021/bi500059y | *Biochemistry* 2014, 53, 4323−4333

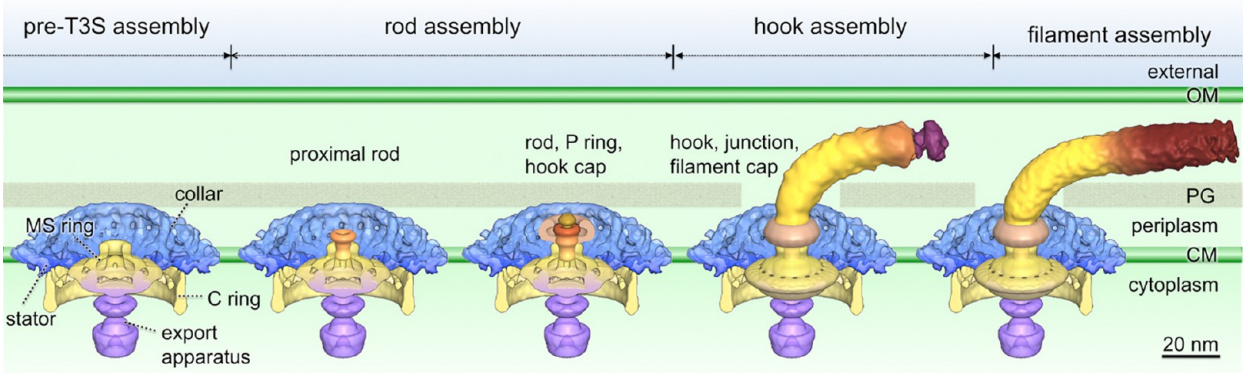

Figure 5. Sequential flagellar assembly process revealed in *B. burgdorferi*.[50] In the pre-T3S assembly state, most flagellar motor components except for the flagellar rod have been assembled, which includes the MS ring, the C ring, the stators, the export apparatus, and the unique periplasmic structure collar. The secretion channel in the MS ring is closed (first panel). The exportation of rod substrates opens the channel, and proximal rod substrates [FliE, FlgB, FlgC, and FlhO (FlgF homologue)] cooperatively assemble into a stable proximal rod structure (second panel). The distal rod protein FlgG adds onto the proximal rod and polymerizes until it reaches a determined length. With the completion of rod assembly, the hook cap is exported and the P ring is assembled around the rod (third panel). The hook assembly is promoted by a hook cap.[83] With the completion of hook assembly, the hook–filament junction and filament cap are exported (fourth panel). The filament assembly is promoted by the filament cap (fifth panel).[82]

they are anchored to the peptidoglycan layer through the periplasmic domain of MotB. Strikingly, many bacterial species evolve the periplasmic features (Figure 4B–F, colored cyan), in comparison with the *E. coli* motor (Figure 4A). Some external flagella contain a disklike structure (Figure 4B,C).[49] In spirochetes, a periplasmic collar assembles around the MS ring, and these structures appear to be quite heterogeneous in the different spirochetal genera (Figure 4D–F). The function(s) and protein composition of the collar structures are currently unknown. Interestingly, these periplasmic features are closely associated with the stator, suggesting that the stator interacts with the collar. In contrast, the motor structure derived from *E. coli* or *S. enterica* cells does not contain any apparent periplasmic features other than the rod and P and L rings (Figure 4A). The stator complexes in these organisms are known to have variable occupancy and a dynamic nature in their flagellar motors,[74] which may contribute to the lack of a clearly defined stator structure in cryo-ET images.[49]

Overall, cryo-ET images of the core structures (MS ring, rod, and C ring) of spirochetal flagella are similar to those of other bacteria. However, spirochetes also have a clearly discernible stator structure, a spirochete-specific collar, and variable P and L rings. The small cell diameter (0.1–0.3 μm) and orderly arrangement of flagellar motors near the cell ends in spirochetes also facilitate *in situ* cryo-ET analysis of these structures at 3.5 nm resolution,[52] indicating the benefits of these cells in cryo-ET analysis. The intact flagellar motor structure of *E. coli* recently determined by cryo-ET has a relatively low resolution (5.9 nm).[49] It is likely that further improvement of the cryo-ET resolution can be achieved through the use of minicells,[75−78] high-efficiency electron detectors,[64,65] and high-throughput techniques.[50,79] Nevertheless, spirochetes (*B. burgdorferi* in particular) represent a valuable model system for elucidating key questions in flagellar structure and function.

SEQUENTIAL ASSEMBLY OF BACTERIAL FLAGELLA

Flagellar assembly is a finely orchestrated biochemical process involving both highly regulated motility gene expression and ordered protein assembly.[30,80,81] The morphogenetic pathway for flagellar synthesis has been well-established in *S. enterica*.[82−84] Recently, the combination of cryo-ET and genetic analysis in *B. burgdorferi* has permitted determination of the location of specific flagellar proteins[48,49,52] and the visualization of the process of flagellar assembly in cells. As an example, key intermediates in the flagellar assembly of *B. burgdorferi* can be genetically trapped by systematically targeting individual flagellar genes (encoding the rod, hook, and filament proteins)[50] (Figure 5). Interestingly, the MS ring channel appeared to be closed in a Δ*fliE* mutant, and no rod-associated density was visualized; thus, assembly of the rod in *B. burgdorferi* is FliE-dependent, consistent with studies conducted with *S. enterica*.[71] Cryo-ET analysis of each rod mutant (Δ*fliE*, Δ*flgB*, Δ*flgC*, Δ*flhO*, and Δ*flgG*) permitted assessment of the contribution of each rod protein to rod assembly.[50] Similarly, analysis of hook mutant Δ*flgE* revealed a structure thought to represent a hook cap attached to the end of distal rod. Examination of a *flaB* filament deletion mutant also exhibited a filament cap structure, which is likely related to the cap protein FliD. In this study, high-throughput cryo-ET procedures permitted the comparative analysis of seven flagellar mutants and more than 20000 gigabytes of data and thereby provide a large set of 3D flagellar structures, which may represent key intermediates during flagellar assembly (Figure 5).[50]

ASYMMETRIC RECONSTRUCTION REVEALS NOVEL ARCHITECTURAL ELEMENTS OF THE EXPORT APPARATUS

The flagellar motor is composed of many different components, and each component has its own symmetries.[43] In spirochetes, the periplasmic collar has 16-fold symmetry, while the export apparatus is expected to possess different symmetries.[28,48] To better understand the structure of the export apparatus, we chose the *L. interrogans* motor as an example for further image analysis, because of its striking structural details as shown in Figure 4F. A novel procedure in which specific substructures of interest are classified and aligned without applying rotational symmetry was utilized recently to delineate asymmetric structural assemblies in bacteriophage T7.[79] This approach, which avoids introducing potential artifactual periodicities and thus obscuring "true" symmetries, was used to determine the

dx.doi.org/10.1021/bi500059y | *Biochemistry* 2014, 53, 4323–4333

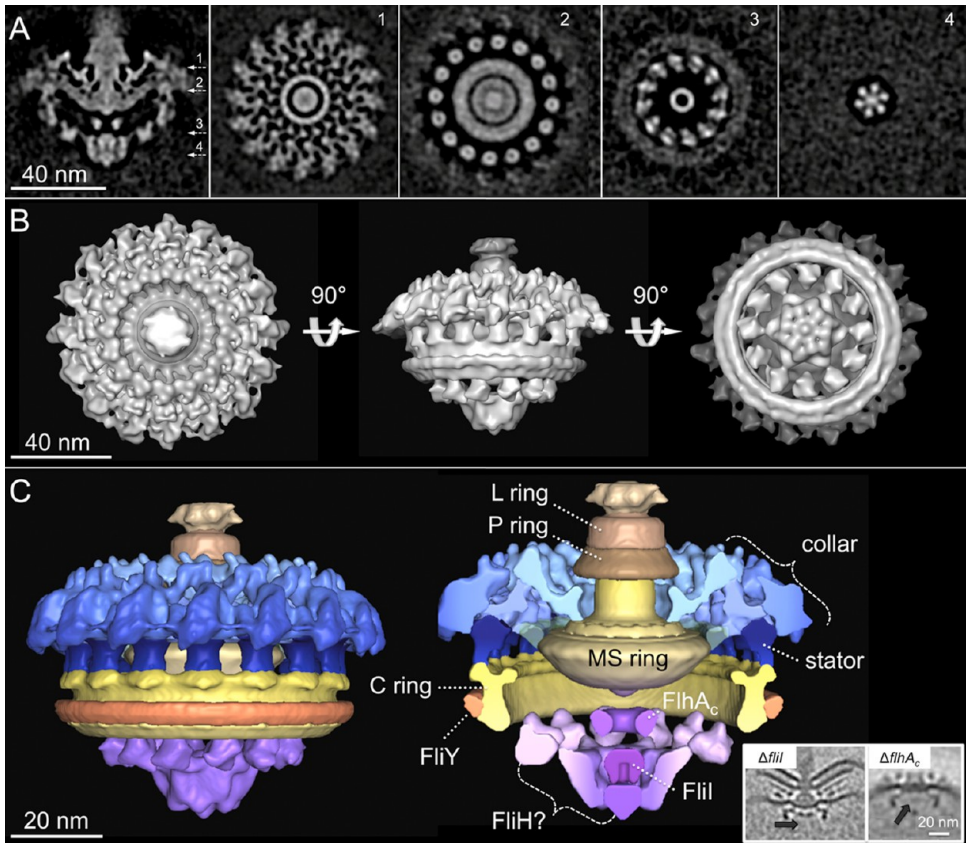

Figure 6. Asymmetric reconstruction of the *L. interrogans* flagellar motor. A central section of the asymmetric reconstruction is shown in panel A. Panels 1−4 are horizontal cross sections. The locations of the sections are indicated in panel A. Panels 1 and 2 are the putative collar and stator units with 16-fold symmetry. Panels 3 and 4 are the export apparatus with 12- and 6-fold symmetry, respectively. (B) 3D surface rendering of the intact motor displayed in three different views. (C) Segmentation of the motor according to the previous density outline. The complex structures inside the C ring are ascribed to be the export apparatus. The major components (FliI and FlhA$_C$) of the export apparatus in *C. jejuni* have been identified by *fliI* deletion and *flhA* cytoplasmic domain truncation mutants,[48] as shown in the insets at the bottom right of panel C. The protein densities are colored black, and the lacking densities of FliI and FlhA$_C$ are indicated by black arrows.

structure of the *Leptospira* motor in greater detail (Figure 6). Specifically, classification focusing on the export apparatus revealed significant details in its overall structure and interaction with the C ring (Figure 6A,B). The cytoplasmic portion of the export apparatus complex shows evident features in 6-fold symmetry or 12-fold symmetry, while the periplasmic collar and stator complexes maintain 16-fold symmetry (Figure 6A,B).

According to the structural comparison among different species of flagellar motors, the motor structure of *L. interrogans* can be segmented into several substructures (Figure 6C). The collar is a large and complex periplasmic structure that is anchored on the cytoplasmic membrane and the MS ring. Underneath the membrane, 16 ringlike particles are localized around the MS ring (Figure 6A, panel 2) and likely correspond to the stator complexes;[51] further genetic mutation of the stator is required to define the exact structure and location of the stator. The C ring of *L. interrogans* exhibits an interesting feature of an extra structure attached to the bottom of the C ring (Figure 6C).

The large cytoplasmic structures inside the C ring are recognized as the export apparatus. Genome sequencing of phylogenetically diverse organisms has shown the eight proteins (FliH, FliI, FliJ, FliP, FliQ, FliR, FlhA, and FlhB) that make up of the flagellar export apparatus and are considerably conserved.[72] FlhA is the largest export apparatus protein, which is predicted to have eight transmembrane helices followed by a large cytoplasmic domain. The cytoplasmic domains of nine copies of FlhA likely form this doughnut-shaped ring below the membrane[48] (Figures 4 and 6C). Underneath the FlhA$_C$ ring, a spherical density with a diameter of ∼10 nm is observed in most intact motors (Figure 4). This structure has been hypothesized to be the ATPase FliI, as further substantiated in studies of a Δ*fliI* mutant constructed in *C. jejuni*.[49] FliI is a member of the ATPase family and is thought to form a spherical hexamer for protein export.[26−28] The structures of FlhA and FliI not only are conserved in flagellar motors but also have structural homologues in type III injectisomes, as recently revealed by *in situ* analysis.[77,85] Conserved structures of the FlhA$_C$ ring and FliI ATPase are observed in the flagellar motor of *L. interrogans* (Figure 6C). Importantly, there are novel "linkerlike" structures with six copies in the inner part and 12 copies in the outer part that extend radially to the bottom of the C ring. The overall architecture of the export apparatus is similar to that in F- and V-type ATPase.[31,32] It is also consistent with the biochemical data that show that the FliH/FliI/FliJ complex interacts with both the FlhA ring and the C ring in a comprehensive manner.[86,87] Clearly, the detailed structure of the export apparatus and its secretion mechanisms will be a fascinating topic in the future.

dx.doi.org/10.1021/bi500059y | *Biochemistry* 2014, 53, 4323−4333

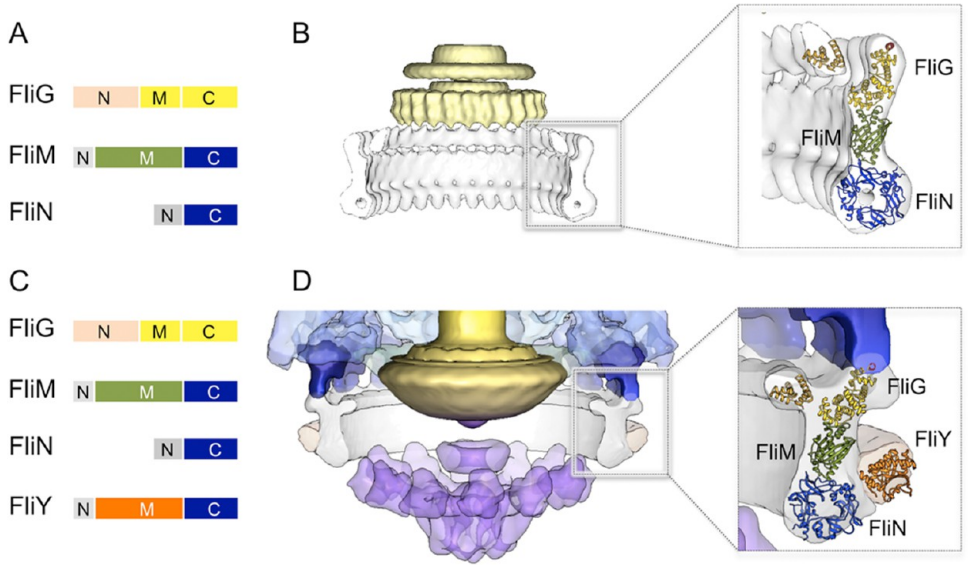

Figure 7. Molecular architecture of the switching complex. (A) Domain organization of the switching complex in *S. enterica*: FliG, FliM, and FliN. (B) Atomic models of $FliG_N$ (PDB-3hjl), the $FliG_{MC}$–$FliM_M$ complex (PDB-4fhr), and FliN (PDB-1yab) were fit in the EM density map of *S. enterica* as described previously.[39] (C) Domain organization of the switching complex in *L. interrogans*: FliG, FliM, FliN, and FliY. The FliY middle domain is homologous to the middle domain of FliM. The C-terminal domain of FliY resembles FliN. (D) The atomic models of FliN, the $FliM_M$–$FliG_{MC}$ complex, and $FliG_N$ were docked into the C ring map of *L. interrogans* as a rigid body. The atomic model of $FliY_M$ (PDB-4hyn) was fit into the extra density on the C ring.

■ ARCHITECTURE OF THE SWITCH COMPLEX

The C ring is known as the switch complex, which plays a crucial role in flagellar switch, assembly, and rotation. FliG is directly involved in the rotor–stator interaction,[23] while FliM and FliN interact with the signaling protein phosphorylated CheY (CheY-P) to regulate switching between CCW and CW rotation.[88−90] Atomic structural information is now available for all components of the switch complex, including the full-length or fragmented FliG,[35−37] FliM,[34] FliN fragments,[38] and the complex of FliG/FliM fragments.[39,40] Together with intact C ring structures determined by cryo-EM and more recently by cryo-ET, these high-resolution structures become the building blocks for achieving a pseudoatomic model of the C ring.

A consensus about the relative positions and orientation of FliM and FliN has been reached, while the difference among models of the C ring is the location of the N- and C-terminal domains of FliG.[35,36,39,40,43] FliN is organized in doughnut-shaped tetramers,[91] which fit well into the bulge density at the bottom of the C ring. A recent crystal structure of the $FliM_M$–$FliG_{MC}$ complex from *Thermotoga maritima* (PDB-4FHR) fits well into the upper density above FliN with the charged helix on $FliG_C$ facing upward (Figure 7B).[39] Importantly, the structures of individual domain structures within the complex are similar to those seen in other crystal structures.[40] The $FliG_M$–$FliM_M$ interface within the crystal structure is consistent with the well-defined hydrophobic interaction between residues of the EHPQR motif in $FliG_M$ and the GGXG motif in $FliM_M$.[92,93] The globular N-terminal domain of FliG from *Aquifex aeolicus*[36] can also be fit to the inner lobe density of the C ring. This model is consistent with the biochemical data that show that the C-terminal domain of FliG ($FliG_C$) interacts with the stator protein MotA while the N-terminal domain of FliG interacts with the C-terminal domain of FliF.[94−96]

The C ring in many different species is in a conformation similar to that in *S. enterica* (Figure 4). However, the C ring in *Leptospira* appears to be strikingly different from others (Figure 4). Apart from the apparent extra density at the bottom of the C ring, the orientation of the upper portion is also different. Similar to those of *Bacillus subtilis* and *T. maritima*, the genome of *L. interrogans* contains two independent genes, *fliY* and *fliN*, while there is no *fliY* in *S. enterica* or *B. burgdorferi*. FliY is a flagellar protein in the CheC phosphatase family.[97] The recent crystal structure[97] of the FliY middle domain fits well into the extra density (Figure 7D), suggesting that FliY is closely associated with the C ring. FliY binding likely plays a critical role in the conformational changes of the switch complex that ultimately lead to the reversal of the direction of rotation. Clearly, further study is needed to understand FliY and its impact on the switch complex and flagellar switch.

■ CONCLUDING REMARKS

The bacterial flagellum is one of the most thoroughly studied prokaryotic motility organelles. Our understanding of this molecular machine has advanced dramatically over the past several decades. More atomic structures of flagellar components are emerging. However, the structure and function of the intact flagellar motor are far from fully understood at the molecular level. Many novel flagellar proteins and other motility-related proteins (YcgR, CheY-P, etc.) are often associated with the conserved core components,[88,89,98] increasing the complexity of the flagellar structure and function. The emergence of cryo-ET and subtomogram averaging provide new avenues for studying intact flagellar motors in cells with unprecedented detail. It is expected that significant advances in cryo-ET, in combination with subtomogram averaging and molecular tools, will provide novel structural insights into many important processes of bacterial flagella: the stator–rotor interaction, protein secretion and assembly, and switching and rotation.

dx.doi.org/10.1021/bi500059y | *Biochemistry* 2014, 53, 4323−4333

AUTHOR INFORMATION

Corresponding Author

*Department of Pathology and Laboratory Medicine, University of Texas Medical School at Houston, Houston, TX 77030. E-mail: jun.liu.1@uth.tmc.edu. Phone: (713) 500-5342. Fax: (713) 500-0730.

Funding

The authors' work in this area has been supported by Grant R01 AI087946 from the National Institute of Allergy and Infectious Diseases and AU-1714 from the Welch Foundation.

Notes

The authors declare no competing financial interest.

REFERENCES

(1) Jarrell, K. F., and McBride, M. J. (2008) The surprisingly diverse ways that prokaryotes move. *Nat. Rev. Microbiol. 6*, 466−476.

(2) Hazelbauer, G. L., Falke, J. J., and Parkinson, J. S. (2008) Bacterial chemoreceptors: High-performance signaling in networked arrays. *Trends Biochem. Sci. 33*, 9−19.

(3) Wadhams, G. H., and Armitage, J. P. (2004) Making sense of it all: Bacterial chemotaxis. *Nat. Rev. Mol. Cell Biol. 5*, 1024−1037.

(4) Berg, H. C. (2003) The rotary motor of bacterial flagella. *Annu. Rev. Biochem. 72*, 19−54.

(5) Charon, N. W., and Goldstein, S. F. (2002) Genetics of motility and chemotaxis of a fascinating group of bacteria: The spirochetes. *Annu. Rev. Genet. 36*, 47−73.

(6) Sze, C. W., Morado, D. R., Liu, J., Charon, N. W., Xu, H., and Li, C. (2011) Carbon storage regulator A (CsrA(Bb)) is a repressor of *Borrelia burgdorferi* flagellin protein FlaB. *Mol. Microbiol. 82*, 851−864.

(7) Motaleb, M. A., Corum, L., Bono, J. L., Elias, A. F., Rosa, P., Samuels, D. S., and Charon, N. W. (2000) *Borrelia burgdorferi* periplasmic flagella have both skeletal and motility functions. *Proc. Natl. Acad. Sci. U.S.A. 97*, 10899−10904.

(8) Sal, M. S., Li, C., Motalab, M. A., Shibata, S., Aizawa, S., and Charon, N. W. (2008) *Borrelia burgdorferi* uniquely regulates its motility genes and has an intricate flagellar hook-basal body structure. *J. Bacteriol. 190*, 1912−1921.

(9) Li, C., Xu, H., Zhang, K., and Liang, F. T. (2010) Inactivation of a putative flagellar motor switch protein FliG1 prevents *Borrelia burgdorferi* from swimming in highly viscous media and blocks its infectivity. *Mol. Microbiol. 75*, 1563−1576.

(10) Charon, N. W., Cockburn, A., Li, C., Liu, J., Miller, K. A., Miller, M. R., Motaleb, M. A., and Wolgemuth, C. W. (2012) The unique paradigm of spirochete motility and chemotaxis. *Annu. Rev. Microbiol. 66*, 349−370.

(11) Macnab, R. M. (2003) How bacteria assemble flagella. *Annu. Rev. Microbiol. 57*, 77−100.

(12) Kojima, S., and Blair, D. F. (2004) The bacterial flagellar motor: Structure and function of a complex molecular machine. *Int. Rev. Cytol. 233*, 93−134.

(13) Sowa, Y., and Berry, R. M. (2008) Bacterial flagellar motor. *Q. Rev. Biophys. 41*, 103−132.

(14) Terashima, H., Kojima, S., and Homma, M. (2008) Flagellar motility in bacteria structure and function of flagellar motor. *Int. Rev. Cell Mol. Biol. 270*, 39−85.

(15) Zhou, J., Fazzio, R. T., and Blair, D. F. (1995) Membrane topology of the MotA protein of *Escherichia coli*. *J. Mol. Biol. 251*, 237−242.

(16) Zhou, J., Lloyd, S. A., and Blair, D. F. (1998) Electrostatic interactions between rotor and stator in the bacterial flagellar motor. *Proc. Natl. Acad. Sci. U.S.A. 95*, 6436−6441.

(17) Chun, S. Y., and Parkinson, J. S. (1988) Bacterial motility: Membrane topology of the *Escherichia coli* MotB protein. *Science 239*, 276−278.

(18) De Mot, R., and Vanderleyden, J. (1994) The C-terminal sequence conservation between OmpA-related outer membrane proteins and MotB suggests a common function in both gram-positive and gram-negative bacteria, possibly in the interaction of these domains with peptidoglycan. *Mol. Microbiol. 12*, 333−334.

(19) Braun, T. F., Al-Mawsawi, L. Q., Kojima, S., and Blair, D. F. (2004) Arrangement of core membrane segments in the MotA/MotB proton-channel complex of *Escherichia coli*. *Biochemistry 43*, 35−45.

(20) Kim, E. A., Price-Carter, M., Carlquist, W. C., and Blair, D. F. (2008) Membrane segment organization in the stator complex of the flagellar motor: Implications for proton flow and proton-induced conformational change. *Biochemistry 47*, 11332−11339.

(21) Braun, T. F., and Blair, D. F. (2001) Targeted disulfide cross-linking of the MotB protein of *Escherichia coli*: Evidence for two H^+ channels in the stator complex. *Biochemistry 40*, 13051−13059.

(22) Zhou, J., Sharp, L. L., Tang, H. L., Lloyd, S. A., Billings, S., Braun, T. F., and Blair, D. F. (1998) Function of protonatable residues in the flagellar motor of *Escherichia coli*: A critical role for Asp 32 of MotB. *J. Bacteriol. 180*, 2729−2735.

(23) Kojima, S., and Blair, D. F. (2001) Conformational change in the stator of the bacterial flagellar motor. *Biochemistry 40*, 13041−13050.

(24) Minamino, T., and Namba, K. (2008) Distinct roles of the FliI ATPase and proton motive force in bacterial flagellar protein export. *Nature 451*, 485−488.

(25) Paul, K., Erhardt, M., Hirano, T., Blair, D. F., and Hughes, K. T. (2008) Energy source of flagellar type III secretion. *Nature 451*, 489−492.

(26) Fan, F., and Macnab, R. M. (1996) Enzymatic characterization of FliI. An ATPase involved in flagellar assembly in *Salmonella typhimurium*. *J. Biol. Chem. 271*, 31981−31988.

(27) Claret, L., Calder, S. R., Higgins, M., and Hughes, C. (2003) Oligomerization and activation of the FliI ATPase central to bacterial flagellum assembly. *Mol. Microbiol. 48*, 1349−1355.

(28) Imada, K., Minamino, T., Tahara, A., and Namba, K. (2007) Structural similarity between the flagellar type III ATPase FliI and F1-ATPase subunits. *Proc. Natl. Acad. Sci. U.S.A. 104*, 485−490.

(29) Erhardt, M., Namba, K., and Hughes, K. T. (2010) Bacterial nanomachines: The flagellum and type III injectisome. *Cold Spring Harbor Perspect. Biol. 2*, a000299.

(30) Macnab, R. M. (2004) Type III flagellar protein export and flagellar assembly. *Biochim. Biophys. Acta 1694*, 207−217.

(31) Ibuki, T., Imada, K., Minamino, T., Kato, T., Miyata, T., and Namba, K. (2011) Common architecture of the flagellar type III protein export apparatus and F- and V-type ATPases. *Nat. Struct. Mol. Biol. 18*, 277−282.

(32) Pallen, M. J., Bailey, C. M., and Beatson, S. A. (2006) Evolutionary links between FliH/YscL-like proteins from bacterial type III secretion systems and second-stalk components of the FoF1 and vacuolar ATPases. *Protein Sci. 15*, 935−941.

(33) Samatey, F. A., Imada, K., Nagashima, S., Vonderviszt, F., Kumasaka, T., Yamamoto, M., and Namba, K. (2001) Structure of the bacterial flagellar protofilament and implications for a switch for supercoiling. *Nature 410*, 331−337.

(34) Park, S. Y., Lowder, B., Bilwes, A. M., Blair, D. F., and Crane, B. R. (2006) Structure of FliM provides insight into assembly of the switch complex in the bacterial flagella motor. *Proc. Natl. Acad. Sci. U.S.A. 103*, 11886−11891.

(35) Minamino, T., Imada, K., Kinoshita, M., Nakamura, S., Morimoto, Y. V., and Namba, K. (2011) Structural insight into the rotational switching mechanism of the bacterial flagellar motor. *PLoS Biol. 9*, e1000616.

(36) Lee, L. K., Ginsburg, M. A., Crovace, C., Donohoe, M., and Stock, D. (2010) Structure of the torque ring of the flagellar motor and the molecular basis for rotational switching. *Nature 466*, 996−1000.

(37) Brown, P. N., Hill, C. P., and Blair, D. F. (2002) Crystal structure of the middle and C-terminal domains of the flagellar rotor protein FliG. *EMBO J. 21*, 3225−3234.

(38) Brown, P. N., Mathews, M. A., Joss, L. A., Hill, C. P., and Blair, D. F. (2005) Crystal structure of the flagellar rotor protein FliN from *Thermotoga maritima*. *J. Bacteriol. 187*, 2890−2902.

(39) Vartanian, A. S., Paz, A., Fortgang, E. A., Abramson, J., and Dahlquist, F. W. (2012) Structure of flagellar motor proteins in complex allows for insights into motor structure and switching. *J. Biol. Chem. 287*, 35779−35783.
(40) Paul, K., Gonzalez-Bonet, G., Bilwes, A. M., Crane, B. R., and Blair, D. (2011) Architecture of the flagellar rotor. *EMBO J. 30*, 2962−2971.
(41) Roujeinikova, A. (2008) Crystal structure of the cell wall anchor domain of MotB, a stator component of the bacterial flagellar motor: Implications for peptidoglycan recognition. *Proc. Natl. Acad. Sci. U.S.A. 105*, 10348−10353.
(42) Kojima, S., Imada, K., Sakuma, M., Sudo, Y., Kojima, C., Minamino, T., Homma, M., and Namba, K. (2009) Stator assembly and activation mechanism of the flagellar motor by the periplasmic region of MotB. *Mol. Microbiol. 73*, 710−718.
(43) Thomas, D. R., Francis, N. R., Xu, C., and DeRosier, D. J. (2006) The three-dimensional structure of the flagellar rotor from a clockwise-locked mutant of *Salmonella enterica serovar Typhimurium*. *J. Bacteriol. 188*, 7039−7048.
(44) Coulton, J. W., and Murray, R. G. (1978) Cell envelope associations of *Aquaspirillum serpens* flagella. *J. Bacteriol. 136*, 1037−1049.
(45) Khan, S., Dapice, M., and Reese, T. S. (1988) Effects of *mot* gene expression on the structure of the flagellar motor. *J. Mol. Biol. 202*, 575−584.
(46) Katayama, E., Shiraishi, T., Oosawa, K., Baba, N., and Aizawa, S. (1996) Geometry of the flagellar motor in the cytoplasmic membrane of *Salmonella typhimurium* as determined by stereo-photogrammetry of quick-freeze deep-etch replica images. *J. Mol. Biol. 255*, 458−475.
(47) Murphy, G. E., Leadbetter, J. R., and Jensen, G. J. (2006) *In situ* structure of the complete *Treponema primitia* flagellar motor. *Nature 442*, 1062−1064.
(48) Abrusci, P., Vergara-Irigaray, M., Johnson, S., Beeby, M. D., Hendrixson, D. R., Roversi, P., Friede, M. E., Deane, J. E., Jensen, G. J., Tang, C. M., and Lea, S. M. (2013) Architecture of the major component of the type III secretion system export apparatus. *Nat. Struct. Mol. Biol. 20*, 99−104.
(49) Chen, S., Beeby, M., Murphy, G. E., Leadbetter, J. R., Hendrixson, D. R., Briegel, A., Li, Z., Shi, J., Tocheva, E. I., Muller, A., Dobro, M. J., and Jensen, G. J. (2011) Structural diversity of bacterial flagellar motors. *EMBO J. 30*, 2972−2981.
(50) Zhao, X., Zhang, K., Boquoi, T., Hu, B., Motaleb, M. A., Miller, K. A., James, M. E., Charon, N. W., Manson, M. D., Norris, S. J., Li, C., and Liu, J. (2013) Cryoelectron tomography reveals the sequential assembly of bacterial flagella in *Borrelia burgdorferi*. *Proc. Natl. Acad. Sci. U.S.A. 110*, 14390−14395.
(51) Raddi, G., Morado, D. R., Yan, J., Haake, D. A., Yang, X. F., and Liu, J. (2012) Three-dimensional structures of pathogenic and saprophytic Leptospira species revealed by cryo-electron tomography. *J. Bacteriol. 194*, 1299−1306.
(52) Liu, J., Lin, T., Botkin, D. J., McCrum, E., Winkler, H., and Norris, S. J. (2009) Intact flagellar motor of *Borrelia burgdorferi* revealed by cryo-electron tomography: Evidence for stator ring curvature and rotor/C-ring assembly flexion. *J. Bacteriol. 191*, 5026−5036.
(53) Motaleb, M. A., Pitzer, J. E., Sultan, S. Z., and Liu, J. (2011) A novel gene inactivation system reveals altered periplasmic flagellar orientation in a *Borrelia burgdorferi* fliL mutant. *J. Bacteriol. 193*, 3324−3331.
(54) Frank, J. (2006) *Electron tomography: Methods for three-dimensional visualization of structures in the cell*, 2nd ed., Springer, New York.
(55) Briggs, J. A. (2013) Structural biology in situ: The potential of subtomogram averaging. *Curr. Opin. Struct. Biol. 23*, 261−267.
(56) Liu, J., Wright, E. R., and Winkler, H. (2010) 3D visualization of HIV virions by cryoelectron tomography. *Methods Enzymol. 483*, 267−290.
(57) Winkler, H. (2007) 3D reconstruction and processing of volumetric data in cryo-electron tomography. *J. Struct. Biol. 157*, 126−137.
(58) Gan, L., and Jensen, G. J. (2012) Electron tomography of cells. *Q. Rev. Biophys. 45*, 27−56.
(59) Lucic, V., Rigort, A., and Baumeister, W. (2013) Cryo-electron tomography: The challenge of doing structural biology in situ. *J. Cell Biol. 202*, 407−419.
(60) Zheng, S. Q., Sedat, J. W., and Agard, D. A. (2010) Automated data collection for electron microscopic tomography. *Methods Enzymol. 481*, 283−315.
(61) Fernandez, J. J. (2012) Computational methods for electron tomography. *Micron 43*, 1010−1030.
(62) Danev, R., Kanamaru, S., Marko, M., and Nagayama, K. (2010) Zernike phase contrast cryo-electron tomography. *J. Struct. Biol. 171*, 174−181.
(63) Hosogi, N., Shigematsu, H., Terashima, H., Homma, M., and Nagayama, K. (2011) Zernike phase contrast cryo-electron tomography of sodium-driven flagellar hook-basal bodies from *Vibrio alginolyticus*. *J. Struct. Biol. 173*, 67−76.
(64) Bai, X. C., Fernandez, I. S., McMullan, G., and Scheres, S. H. (2013) Ribosome structures to near-atomic resolution from thirty thousand cryo-EM particles. *eLife 2*, e00461.
(65) Li, X., Mooney, P., Zheng, S., Booth, C. R., Braunfeld, M. B., Gubbens, S., Agard, D. A., and Cheng, Y. (2013) Electron counting and beam-induced motion correction enable near-atomic-resolution single-particle cryo-EM. *Nat. Methods 10*, 584−590.
(66) Francis, N. R., Sosinsky, G. E., Thomas, D., and DeRosier, D. J. (1994) Isolation, characterization and structure of bacterial flagellar motors containing the switch complex. *J. Mol. Biol. 235*, 1261−1270.
(67) Suzuki, H., Yonekura, K., and Namba, K. (2004) Structure of the rotor of the bacterial flagellar motor revealed by electron cryomicroscopy and single-particle image analysis. *J. Mol. Biol. 337*, 105−113.
(68) Kudryashev, M., Cyrklaff, M., Wallich, R., Baumeister, W., and Frischknecht, F. (2010) Distinct in situ structures of the *Borrelia* flagellar motor. *J. Struct. Biol. 169*, 54−61.
(69) Homma, M., Kutsukake, K., Hasebe, M., Iino, T., and Macnab, R. M. (1990) FlgB, FlgC, FlgF and FlgG. A family of structurally related proteins in the flagellar basal body of *Salmonella typhimurium*. *J. Mol. Biol. 211*, 465−477.
(70) Jones, C. J., and Macnab, R. M. (1990) Flagellar assembly in *Salmonella typhimurium*: Analysis with temperature-sensitive mutants. *J. Bacteriol. 172*, 1327−1339.
(71) Minamino, T., Yamaguchi, S., and Macnab, R. M. (2000) Interaction between FliE and FlgB, a proximal rod component of the flagellar basal body of *Salmonella*. *J. Bacteriol. 182*, 3029−3036.
(72) Pallen, M. J., Penn, C. W., and Chaudhuri, R. R. (2005) Bacterial flagellar diversity in the post-genomic era. *Trends Microbiol. 13*, 143−149.
(73) Liu, J., Howell, J. K., Bradley, S. D., Zheng, Y., Zhou, Z. H., and Norris, S. J. (2010) Cellular architecture of *Treponema pallidum*: Novel flagellum, periplasmic cone, and cell envelope as revealed by cryo electron tomography. *J. Mol. Biol. 403*, 546−561.
(74) Leake, M. C., Chandler, J. H., Wadhams, G. H., Bai, F., Berry, R. M., and Armitage, J. P. (2006) Stoichiometry and turnover in single, functioning membrane protein complexes. *Nature 443*, 355−358.
(75) Briegel, A., Li, X., Bilwes, A. M., Hughes, K. T., Jensen, G. J., and Crane, B. R. (2012) Bacterial chemoreceptor arrays are hexagonally packed trimers of receptor dimers networked by rings of kinase and coupling proteins. *Proc. Natl. Acad. Sci. U.S.A. 109*, 3766−3771.
(76) Liu, J., Chen, C. Y., Shiomi, D., Niki, H., and Margolin, W. (2011) Visualization of bacteriophage P1 infection by cryo-electron tomography of tiny *Escherichia coli*. *Virology 417*, 304−311.
(77) Kudryashev, M., Stenta, M., Schmelz, S., Amstutz, M., Wiesand, U., Castano-Diez, D., Degiacomi, M. T., Munnich, S., Bleck, C. K., Kowal, J., Diepold, A., Heinz, D. W., Dal Peraro, M., Cornelis, G. R., and Stahlberg, H. (2013) In situ structural analysis of the *Yersinia enterocolitica* injectisome. *eLife 2*, e00792.

(78) Liu, J., Hu, B., Morado, D. R., Jani, S., Manson, M. D., and Margolin, W. (2012) Molecular architecture of chemoreceptor arrays revealed by cryoelectron tomography of *Escherichia coli* minicells. *Proc. Natl. Acad. Sci. U.S.A. 109*, E1481−E1488.
(79) Hu, B., Margolin, W., Molineux, I. J., and Liu, J. (2013) The bacteriophage t7 virion undergoes extensive structural remodeling during infection. *Science 339*, 576−579.
(80) Chevance, F. F., and Hughes, K. T. (2008) Coordinating assembly of a bacterial macromolecular machine. *Nat. Rev. Microbiol. 6*, 455−465.
(81) Kubori, T., Shimamoto, N., Yamaguchi, S., Namba, K., and Aizawa, S. (1992) Morphological pathway of flagellar assembly in *Salmonella typhimurium*. *J. Mol. Biol. 226*, 433−446.
(82) Yonekura, K., Maki, S., Morgan, D. G., DeRosier, D. J., Vonderviszt, F., Imada, K., and Namba, K. (2000) The bacterial flagellar cap as the rotary promoter of flagellin self-assembly. *Science 290*, 2148−2152.
(83) Ohnishi, K., Ohto, Y., Aizawa, S., Macnab, R. M., and Iino, T. (1994) FlgD is a scaffolding protein needed for flagellar hook assembly in *Salmonella typhimurium*. *J. Bacteriol. 176*, 2272−2281.
(84) Hirano, T., Minamino, T., and Macnab, R. M. (2001) The role in flagellar rod assembly of the N-terminal domain of *Salmonella* FlgJ, a flagellum-specific muramidase. *J. Mol. Biol. 312*, 359−369.
(85) Kawamoto, A., Morimoto, Y. V., Miyata, T., Minamino, T., Hughes, K. T., Kato, T., and Namba, K. (2013) Common and distinct structural features of *Salmonella* injectisome and flagellar basal body. *Sci. Rep. 3*, 3369.
(86) Minamino, T., Shimada, M., Okabe, M., Saijo-Hamano, Y., Imada, K., Kihara, M., and Namba, K. (2010) Role of the C-terminal cytoplasmic domain of FlhA in bacterial flagellar type III protein export. *J. Bacteriol. 192*, 1929−1936.
(87) Gonzalez-Pedrajo, B., Minamino, T., Kihara, M., and Namba, K. (2006) Interactions between C ring proteins and export apparatus components: A possible mechanism for facilitating type III protein export. *Mol. Microbiol. 60*, 984−998.
(88) Sarkar, M. K., Paul, K., and Blair, D. (2010) Chemotaxis signaling protein CheY binds to the rotor protein FliN to control the direction of flagellar rotation in *Escherichia coli*. *Proc. Natl. Acad. Sci. U.S.A. 107*, 9370−9375.
(89) Dyer, C. M., Vartanian, A. S., Zhou, H., and Dahlquist, F. W. (2009) A molecular mechanism of bacterial flagellar motor switching. *J. Mol. Biol. 388*, 71−84.
(90) Welch, M., Oosawa, K., Aizawa, S., and Eisenbach, M. (1993) Phosphorylation-dependent binding of a signal molecule to the flagellar switch of bacteria. *Proc. Natl. Acad. Sci. U.S.A. 90*, 8787−8791.
(91) Paul, K., and Blair, D. F. (2006) Organization of FliN subunits in the flagellar motor of *Escherichia coli*. *J. Bacteriol. 188*, 2502−2511.
(92) Marykwas, D. L., and Berg, H. C. (1996) A mutational analysis of the interaction between FliG and FliM, two components of the flagellar motor of *Escherichia coli*. *J. Bacteriol. 178*, 1289−1294.
(93) Brown, P. N., Terrazas, M., Paul, K., and Blair, D. F. (2007) Mutational analysis of the flagellar protein FliG: Sites of interaction with FliM and implications for organization of the switch complex. *J. Bacteriol. 189*, 305−312.
(94) Kihara, M., Miller, G. U., and Macnab, R. M. (2000) Deletion analysis of the flagellar switch protein FliG of *Salmonella*. *J. Bacteriol. 182*, 3022−3028.
(95) Grunenfelder, B., Gehrig, S., and Jenal, U. (2003) Role of the cytoplasmic C terminus of the FliF motor protein in flagellar assembly and rotation. *J. Bacteriol. 185*, 1624−1633.
(96) Levenson, R., Zhou, H., and Dahlquist, F. W. (2012) Structural insights into the interaction between the bacterial flagellar motor proteins FliF and FliG. *Biochemistry 51*, 5052−5060.
(97) Sircar, R., Greenswag, A. R., Bilwes, A. M., Gonzalez-Bonet, G., and Crane, B. R. (2013) Structure and activity of the flagellar rotor protein FliY: A member of the CheC phosphatase family. *J. Biol. Chem. 288*, 13493−13502.
(98) Paul, K., Nieto, V., Carlquist, W. C., Blair, D. F., and Harshey, R. M. (2010) The c-di-GMP binding protein YcgR controls flagellar motor direction and speed to affect chemotaxis by a "backstop brake" mechanism. *Mol. Cell 38*, 128−139.